



OPEN

Size and symmetry of the superconducting gap in the f.c.c. Cs_3C_{60} polymorph close to the metal-Mott insulator boundary

Anton Potočnik¹, Andraž Krajnc¹, Peter Jeglič^{1,2}, Yasuhiro Takabayashi³, Alexey Y. Ganin⁴, Kosmas Prassides^{3,6}, Matthew J. Rosseinsky⁴ & Denis Arčon^{1,5}

¹Jožef Stefan Institute, Jamova c. 39, SI-1000 Ljubljana, Slovenia, ²EN-FIST Centre of Excellence, Dunajska c. 156, SI-1000 Ljubljana, Slovenia, ³Department of Chemistry, Durham University, Durham DH1 3LE, UK, ⁴Department of Chemistry, University of Liverpool, Liverpool L69 7ZD, UK, ⁵Faculty of mathematics and physics, University of Ljubljana, Jadranska c. 19, SI-1000 Ljubljana, Slovenia, ⁶WPI Research Center, Advanced Institute for Materials Research, Tohoku University, Sendai 980-8577, Japan.

Received
11 November 2013

Accepted
17 February 2014

Published
3 March 2014

Correspondence and requests for materials should be addressed to D.A. (denis.arcon@ijs.si)

The alkali fullerides, A_3C_{60} (A = alkali metal) are molecular superconductors that undergo a transition to a magnetic Mott-insulating state at large lattice parameters. However, although the size and the symmetry of the superconducting gap, Δ , are both crucial for the understanding of the pairing mechanism, they are currently unknown for superconducting fullerides close to the correlation-driven magnetic insulator. Here we report a comprehensive nuclear magnetic resonance (NMR) study of face-centred-cubic (f.c.c.) Cs_3C_{60} polymorph, which can be tuned continuously through the bandwidth-controlled Mott insulator-metal/superconductor transition by pressure. When superconductivity emerges from the insulating state at large interfullerene separations upon compression, we observe an isotropic (*s*-wave) Δ with a large gap-to-superconducting transition temperature ratio, $2\Delta_0/k_{\text{B}}T_{\text{c}} = 5.3(2)$ [$\Delta_0 = \Delta(0\text{ K})$]. $2\Delta_0/k_{\text{B}}T_{\text{c}}$ decreases continuously upon pressurization until it approaches a value of ~ 3.5 , characteristic of weak-coupling BCS theory of superconductivity despite the dome-shaped dependence of T_{c} on interfullerene separation. The results indicate the importance of the electronic correlations for the pairing interaction as the metal/superconductor-insulator boundary is approached.

The family of unconventional superconductors, that do not fit into the framework of the Bardeen-Cooper-Schrieffer (BCS) theory, has grown considerably over the last couple of decades and now includes cuprates¹, heavy-fermions², organic superconductors³ and most recently also iron pnictides⁴. They all share a similar phase diagram^{5,6} – superconductivity emerges through doping or applied pressure when the competing magnetic state is suppressed. Remarkably, even after more than 20 years of intensive research the superconducting pairing mechanism is still not fully understood for these compounds⁷. However, unlike in the phonon-driven BCS superconductors, strong electron correlations and magnetic interactions are believed to be important for the Cooper pairing mechanism.

A comparable phase diagram has been recently established for the cubic alkali fullerides A_3C_{60} (A = alkali metal)^{8–10} with the unit cell volume per fulleride ion, V , as a controlling parameter. For small V , short distances between neighbouring C_{60}^{3-} anions result in a strong overlap of the highest occupied triply-degenerate t_{1u} molecular orbitals and stabilize a Fermi-liquid metallic state from which the superconductivity emerges^{11,12}. T_{c} at first increases with V but then for the optimal V^{max} it reaches a maximum $T_{\text{c}}^{\text{max}} = 35$ and 38 K for the face-centred (f.c.c.) and A15 cubic polymorphs, respectively^{8–10}. For even larger V , which are accessible only with the Cs_3C_{60} composition under pressure, T_{c} starts to decrease with increasing V . At the critical volume V_{m} , the on-site electron-electron Coulomb repulsion energy (U) prevails over the electronic kinetic energy (measured by the bandwidth W) and the metal/superconductor-to-Mott Jahn Teller-insulator transition (MIT) takes place. The importance of the Jahn-Teller effect arises from the intrinsic orbital degeneracy of the fullerides¹³.

The size and symmetry of the superconducting gap, Δ , characterize the superconducting state. In the case of cuprates, the *d*-wave symmetry of the superconducting gap¹⁴ and its large amplitude ($2\Delta_0/k_{\text{B}}T_{\text{c}}$ is much larger than the weak-coupling BCS value of 3.5^{15,16}; here Δ_0 is the value of Δ extrapolated to 0 K) are considered as fingerprints of an unconventional superconducting state. On the other hand, isotropic (*s*-wave) gaps with

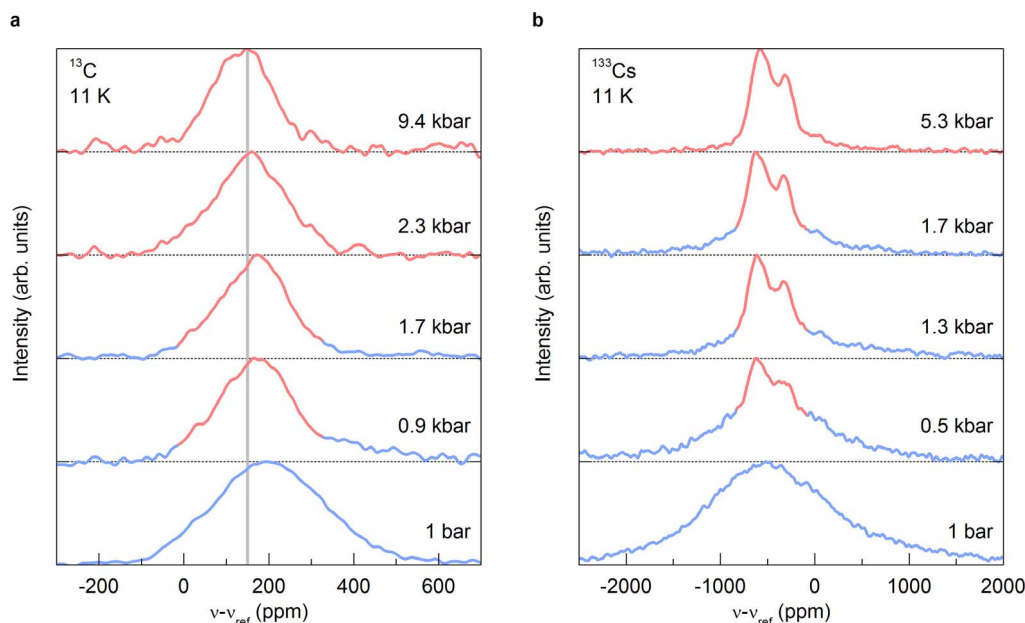


Figure 1 | Phase coexistence. ^{13}C (a) and ^{133}Cs (b) NMR spectra of f.c.c. Cs_3C_{60} measured at 11 K in the superconducting state as a function of pressure. The ^{13}C (^{133}Cs) NMR spectra measured at ambient pressure in the paramagnetic Mott-insulating state are also shown for comparison. At low pressure ($0.5 \leq P \leq 1.3$ kbar), two contributions to the spectrum from the superconducting (red lines) and Mott-insulating (blue lines) phases are present. The grey vertical line in (a) marks the expected (chemical) shift in the superconducting state.

substantially different sizes for different Fermi pockets are found in iron-pnictides¹⁷, where Hund's rules play an important role in controlling the electronic structure¹⁸. Despite these differences, the scaling of Δ_0 with T_c in the underdoped regime in both families^{16,17} suggests that Δ_0 is controlled by the pairing strength. In the case of the extensively studied $A_3\text{C}_{60}$ molecular superconductors with $V < V^{\text{max}}$, such as K_3C_{60} and Rb_3C_{60} , the isotropic Δ found in numerous NMR or μSR experiments^{11,19–22} has been for many years regarded as a result of a standard type-II BCS superconductivity in the weak coupling limit. However, the strong on-site electron-electron repulsion ($U \sim 1$ eV)²³, which is comparable with or even larger than the bandwidth ($W \sim 0.5$ eV)^{11,12}, suggests the importance of electron correlations and casts doubts on the applicability of the BCS formalism²⁴ thus bringing forward models of superconductivity which explicitly include correlations^{25–28}. For $V > V^{\text{max}}$, the decrease of T_c with V found for both polymorphs of Cs_3C_{60} under pressure^{9,10} is a strong indication of the growing importance of electron correlations. Although experiments on expanded Cs_3C_{60} have precisely determined the locations of the superconducting, normal and Mott-insulating states on the phase diagram^{9,10,29–31}, the key information about the size and the symmetry of the superconducting gap in the vicinity of the parent Mott-Jahn-Teller insulating state is still missing.

In this work, we have used the local-probes ^{13}C and ^{133}Cs NMR at high hydrostatic pressures to study the f.c.c. Cs_3C_{60} polymorph as it is driven back from the ambient-pressure Mott-insulating state to a metallic/high- T_c superconducting state by compression. We find that as the pressure is released and V increases, the decrease in T_c in the vicinity of the metal-insulator (MI) boundary is accompanied by the significant enhancement of the superconducting ratio, $2\Delta_0/k_B T_c$ while the s -wave symmetry of the superconducting order parameter is retained for all V . The BCS theory fails to account for these results, which thus provide very stringent tests for the fundamental mechanisms that are responsible for superconductivity in f.c.c. $A_3\text{C}_{60}$.

Results

The high f.c.c. Cs_3C_{60} (86%) phase fraction of the present sample has allowed us to use ^{13}C and ^{133}Cs NMR spectroscopy as a local probe of

the normal and superconducting state properties of the f.c.c. Cs_3C_{60} polymorph with applied pressure (Fig. 1, Fig. S1). At ambient pressure, the large paramagnetic susceptibility of the exchange-coupled Mott-insulating state at low temperature dramatically broadens the NMR spectra through the hyperfine interaction¹⁰ and, for instance, prevents the clear separation of octahedral and tetrahedral ^{133}Cs signals. The ^{13}C NMR shift calculated from the first moment of the spectra, is shifted by about 190 ppm relative to the TMS standard, a characteristic value of C_{60}^{3-} ions (Fig. 1a). At the same time, the ^{13}C spin-lattice relaxation rate (Fig. S2), $1/^{13}T_1$, is temperature independent consistent with the insulating nature of the electronic ground state down to 4 K¹⁰.

Slight pressurization of the sample leads to the appearance in the spectra of an additional much narrower component in addition to the broad NMR signal due to the paramagnetic insulator. In the case of the ^{133}Cs NMR spectra measured at 0.5 and 1.3 kbar (Fig. 1b), this is seen as the emergence of a two-peak component with a peak intensity ratio of 2:1 – reflecting the relative occupancy by the Cs^+ ions of the tetrahedral and octahedral sites³², respectively, in the crystal structure – superimposed on the broad signal. Similarly, the ^{13}C NMR spectra show low-temperature narrowing (Fig. 1a) below approximately 25 K at 0.9 kbar. This narrowing of the NMR spectra with applied pressure provides the signature of the transition to the superconducting state in which the spin susceptibility vanishes, affording the sharper signals which come from the superconductor. The appearance of the superconducting component is also picked up very sensitively in the spin-lattice relaxation rate data (Fig. S2). For instance, slight pressurization ($P = 0.9$ kbar) of the f.c.c. Cs_3C_{60} sample leads to an incomplete suppression of $1/^{13}T_1 T$ below $T_c = 25$ K that is consistent with the opening of the superconducting gap, Δ . However, since $1/^{13}T_1 T$ does not approach zero even when the temperature is reduced well below T_c , the transition here to the superconducting state is incomplete. The partial suppression of the spin-lattice relaxation rates and the presence of two overlapping NMR components are thus consistent with the presence of superconducting and Mott-insulating phases in different parts of the sample at these pressures. Such phase coexistence close to the MIT



boundary has also been detected for the A15 Cs_3C_{60} polymorph⁹ and implies that the transition between the Mott-insulating and superconducting states is of first order.

As the pressure is gradually increased, the narrow NMR signal due to the superconducting component completely dominates the low-temperature NMR spectra in agreement with the presence of bulk superconductivity for $P \geq 1.7$ kbar (Fig. 1). The critical temperature has increased to 26.5(5) K at 1.7 kbar. At this pressure, the temperature dependence of the ^{13}C NMR line shift, calculated from the first moment of the spectra, is rapidly suppressed for $T \leq T_c$ (Fig. 2). We note that in the superconducting state there are three main contributions to the ^{13}C NMR shift: the temperature-independent chemical shift, the Knight shift, which is proportional to the spin susceptibility, and the diamagnetic contribution due to the Meissner effect. The latter is estimated to be very small – around 3.2 ppm³³ – and can thus be neglected. The ^{13}C NMR shift approaches ~ 150 ppm as $T \rightarrow 0$, which is the value expected for the C_{60}^{3-} isotropic chemical shift³³. We thus conclude that the Knight shift vanishes at $T = 0$ thus providing firm evidence for the vanishing spin susceptibility of the spin-singlet Cooper pairs. The complete suppression of the ^{13}C and ^{133}Cs spin-lattice relaxation rates well below T_c also fully supports such a conclusion. However, there is no characteristic enhancement of the spin-lattice relaxation rates just below T_c that would mark the presence of the Hebel-Slichter coherence peak [Fig. 2b & d].

The temperature dependence of the spin-lattice relaxation rates below T_c can provide information on the size and symmetry of the superconducting gap, Δ . Plotting $(1/^{13}\text{T}_1)$ against $1/T$ as a semilog plot for the 1.7 kbar data yields a straight line [Fig. 3a & Fig. S3]. This implies that the temperature dependence of the spin-lattice relaxation rate follows an activated behaviour with a single isotropic BCS-like (*s*-wave) superconducting gap, Δ_0 as described by the equation: $1/^{13}\text{T}_1 \propto \exp[-\Delta_0/k_B T]$, where k_B is the Boltzmann constant. This result rules out other singlet-pairing symmetries, such as that of a *d*-wave for which a power-law dependence $1/^{13}\text{T}_1 \propto T^3$ is expected³⁴. However, at the lowest temperatures, the T_1 values are unambiguously longer by at least a factor of four than those expected in the BCS weak-coupling limit implying strong enhancement of the superconducting gap. Taking into account data for $(T_c/T) > 1.25$, the magnitude of Δ_0 at 1.7 kbar is found to be 6.0(2) meV. At the same time, the normalised gap value, $2\Delta_0/k_B T_c = 5.3(2)$ is significantly enhanced relative to that expected for a weakly coupled BCS superconductor ($2\Delta_0/k_B T_c = 3.52$). The single *s*-wave symmetry superconducting gap in f.c.c. Cs_3C_{60} contrasts with the behaviour of other

high-temperature superconducting families. The cuprates, which have a parent Mott insulating state like the fullerides and are accepted as strongly correlated, universally show *d*-wave superconductivity¹⁴. MgB_2 , which is not correlated and has multiple bands at the Fermi level that can be compared with the three electronically active t_{1u} orbitals in Cs_3C_{60} , is *s*-wave but displays multiple gaps^{35,36}. Similarly, the iron pnictides, which are weakly to moderately correlated systems with multiple bands, also show multiple *s*-wave gap behaviour¹⁸.

Having established the fundamental behaviour of f.c.c. Cs_3C_{60} close to the metal/superconductor-to-insulator transition, we next address how the superconducting gap relates to the superconducting T_c upon tuning the bandwidth by pressure. As the applied pressure increases and the interfullerene separation gradually decreases, T_c (Fig. 3b) first increases (29(1) K at 2.9 kbar), reaches a maximum at 33(1) K at 7.8 kbar and then begins to decrease to 30.5(8) K at the highest pressure of the present experiments (14.2 kbar) tracking the dome-shaped, $T_c(P)$ response established before by low-field magnetisation measurements¹⁰. However, contrary to this behaviour of T_c , the gap, Δ_0 does not show a maximum value but rather decreases monotonically (Fig. S3) with increasing bandwidth (decreasing V). When the normalised value of the gap, $2\Delta_0/k_B T_c = 4.7(2)$ (at 2.9 kbar) is considered (Fig. 3c), we find that this smoothly decreases towards the BCS weak coupling value of 3.52 at 7.8 kbar and above, implying a continuous reduction in the coupling strength as the system moves away from the metal-to-insulator boundary.

Discussion

The enhancement of $2\Delta_0/k_B T_c$ (Fig. 3c) with a concomitant decrease in T_c (Fig. 3b) for the large V region of the phase diagram provides an unprecedented opportunity to test the applicability of the BCS theory in alkali fullerides. In principle, the maximal value, $2\Delta_0/k_B T_c \approx 5$ close to the MIT boundary, could be obtained for strong electron-phonon coupling, but this would require optical or intermolecular phonons ($\omega_{\text{ph}} \sim 100 \text{ cm}^{-1}$)³⁷ to take part in the superconducting pairing mechanism. The weak-coupling BCS value of 3.52 found at high P (small V) can only be obtained by the involvement of the intramolecular phonons ($\omega_{\text{ph}} \sim 1000\text{--}1500 \text{ cm}^{-1}$) in the pairing interaction. The V dependence of $2\Delta_0/k_B T_c$ would thus then require that phonon modes in distinctly different spectral regions are active in different parts of the electronic phase diagram. This is unlikely as the intramolecular phonon modes are always present and cannot be active only in one part of the phase diagram. Therefore, these

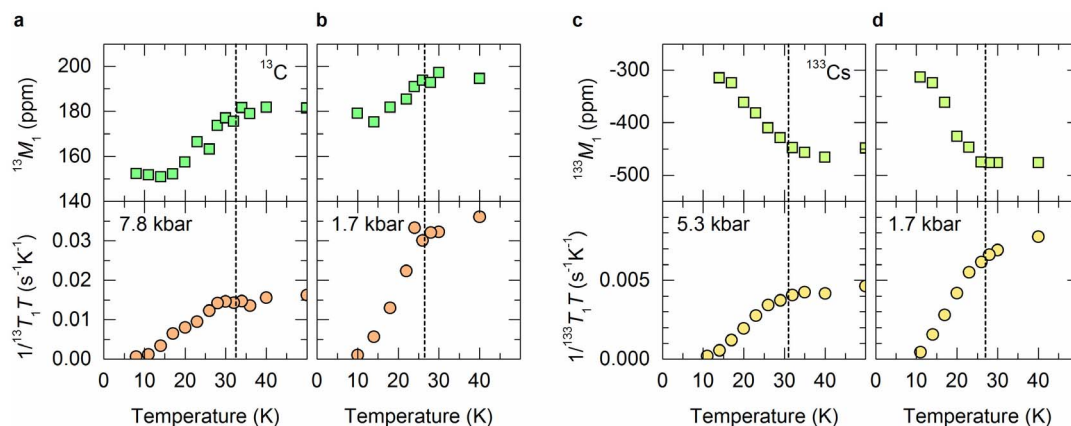


Figure 2 | Critical temperatures. (a), (b) Temperature dependence of the ^{13}C NMR shifts (green squares) and the spin-lattice relaxation rates, $1/^{13}\text{T}_1 T$ (orange circles) measured at 7.8 and 1.7 kbar, respectively. (c), (d) Temperature dependence of the ^{133}Cs NMR shifts (light green squares) and the spin-lattice relaxation rates, $1/^{133}\text{T}_1 T$ (light orange circles) measured at 5.3 and 1.7 kbar, respectively. The ^{13}C (^{133}Cs) NMR shifts were obtained from the first moments, M_1 , of the ^{13}C (^{133}Cs) NMR spectra. The dashed vertical lines mark the onset temperatures at which M_1 becomes suppressed in the superconducting state. At high pressure [(a), (c)], $1/T_1 T$ is suppressed at a slightly lower temperature than M_1 , which is the signature of a damped Hebel-Slichter coherence peak. At low pressure [(b), (d)], the two onset temperatures coincide, thus implying the absence of a coherence peak.

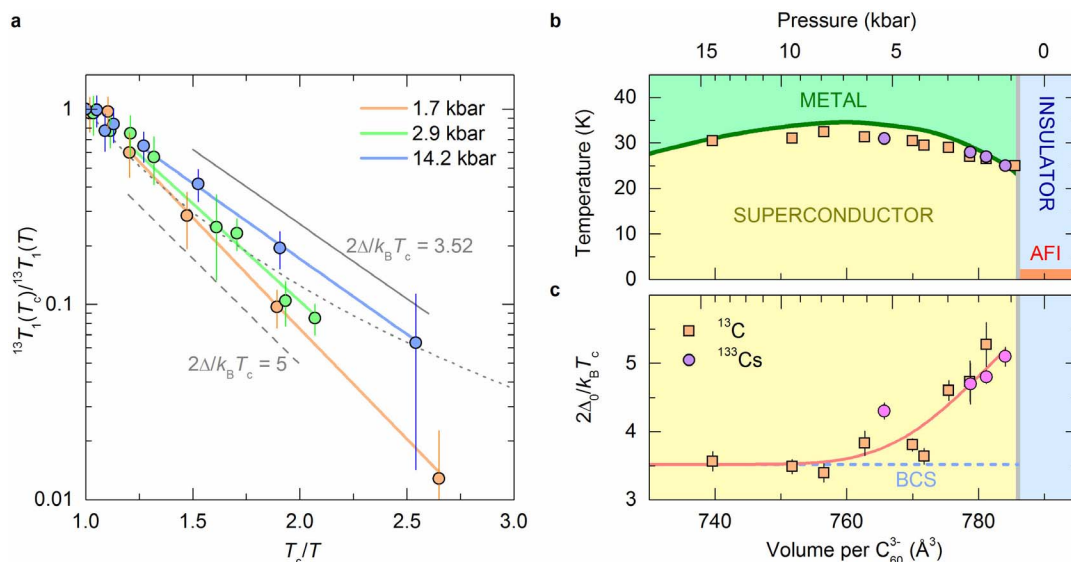


Figure 3 | Superconducting gap. (a) ^{13}C spin-lattice relaxation rate, $1/^{13}T_1$ normalized to its value at T_c vs inverse temperature, T_c/T for three characteristic pressures 1.7 (orange circles), 2.9 (green circles), and 14.2 kbar (blue circles). Solid lines through the points are fits to the equation, $1/^{13}T_1 = A \exp[-\Delta_0/k_B T]$, where the fitting parameters are the amplitude A and the value of the superconducting gap at $T = 0$ K, Δ_0 . Only data for $(T_c/T) > 1.25$ are included in the fits. Thin solid and dashed lines mark the expected slopes for $2\Delta_0/k_B T_c$ ratios of 3.52 and 5, respectively. The dot-dashed line is the power law dependence, $1/^{13}T_1 \propto T^3$ anticipated for d -wave superconductivity. (b) The low-temperature phase diagram of f.c.c. Cs_3C_{60} as derived from the shifts of the NMR spectra in the superconducting state. Squares and circles mark the onset of superconductivity as deduced from the ^{13}C and ^{133}Cs NMR data, respectively. The experiments were conducted at a 9.39 T magnetic field. The volume (pressure, top scale) dependence of T_c represented by the solid green line is that obtained from the low-field magnetization studies on the same sample¹⁰. The thick grey vertical line indicates the critical volume, V_m for the metal/superconductor-to-Mott insulator transition. The antiferromagnetic transition temperature, $T_N = 2.2$ K, of the Mott-insulating phase is taken from Ref. [10] (AFI denotes antiferromagnetic insulating phase). (c) The volume per C_{60}^{3-} , V , dependence of the superconducting gap divided by the superconducting critical temperature, $2\Delta_0/k_B T_c$, obtained from the ^{13}C (squares) and ^{133}Cs (circles) spin-lattice relaxation rate data in the superconducting state. The solid thick line is a guide to the eye, while the dashed blue line marks the BCS value, $2\Delta_0/k_B T_c = 3.52$. The thick grey vertical line marks the metal/superconductor-to-Mott insulator critical volume, V_m .

arguments rule out the conventional BCS-like explanation of superconductivity in f.c.c. Cs_3C_{60} , despite the retention of s -wave symmetry over the entire phase diagram.

The failure of the BCS theory therefore necessitates the presence of an additional parameter responsible for the strong coupling superconductivity as we approach the MIT boundary from the low volume per C_{60}^{3-} , V , side of the phase diagram. In this part of the phase diagram, the screening of the Coulomb interactions is not so effective anymore and the effective U is expected to rapidly increase thus making electron correlations progressively more important. For instance, they are directly reflected in the non-Korringa temperature dependence of $1/T_1 T$ in the normal state for large V ³¹. Therefore, we propose that the additional parameter in the superconducting mechanism is most likely the increased importance of correlations relative to the electronic bandwidth.

The s -wave nature of the superconducting gap and the anomalously large values of $2\Delta_0/k_B T_c$ set the fullerides out as an unusual class of strongly correlated superconductors in which the s -wave nature is retained right across the entire V range but the non-BCS nature is strongly indicated by the V (or bandwidth) dependence of the superconducting gap. This conclusion is in qualitative agreement with the recent application of density functional theory for superconductors within the local density approximation (LDA) to the alkali fullerides, $A_3\text{C}_{60}$ ($A = \text{K}, \text{Rb}, \text{Cs}$)²⁴. This work strongly suggests the necessity to go beyond the framework of the Migdal-Eliashberg theory and calls for direct comparisons with the other families of high-temperature superconductors to determine whether they share the same purely electronic pairing mechanism. In the strongly correlated cuprates, the superconducting gap has a d -wave symmetry in momentum space with the gap values at the “antinodes” that place $2\Delta_0/k_B T_c$ well in the strong coupling regime¹⁵. The gap generally first

increases with doping in the underdoped regime, varying in a similar manner to T_c , but then it soon reaches a maximum and remains at the same size for larger doping levels¹⁶. On the other hand, the pnictides are less correlated systems, but like the fullerides they are multiband superconductors. Their superconducting gaps also scale linearly with T_c in the underdoped regime¹⁷ and show many similarities with the behaviour observed in underdoped cuprates. The opposing volume dependences of $2\Delta_0/k_B T_c$ and T_c observed for the f.c.c. Cs_3C_{60} compound are thus qualitatively different from these two families. Finally, we note that a preprint recently appeared on the arXiv server³⁸ reporting NMR results on the A15 Cs_3C_{60} polymorph that show a comparable V dependence of the superconducting gap thus implying a lattice-independent superconductivity mechanism in both these systems.

Conclusions

The superconducting gap size in f.c.c. Cs_3C_{60} increases as the insulator is approached, but the singlet s -wave nature of the superconductivity is maintained across the entire phase diagram. The observation of a single isotropic gap from a molecular s/p system with three degenerate orbitals contributing to the states at the Fermi energy contrasts with the multiband multigap structure of extreme BCS MgB_2 , which shares the electronic orbital parentage of the states involved but with much broader bands due to its extended non-molecular nature. The weaker overlap between the parent orbitals in the fullerides and the observation of magnetism and electronic correlations in the competing states makes the contrasting variation of Δ_0 and T_c from the cuprates and the pnictides important. Hund’s rules are not relevant for the cuprates, as there is only one accessible spin state with one hole in the parent insulator, but are thought to control the electronic structure of the pnictides²⁰. In the fullerides,



there is a competition between high- and low-spin states involving both Hund's rules and Jahn-Teller electron-phonon coupling, which is decisive in favouring the low-spin state¹³. The observation of a large non-BCS but *s*-wave gap in a superconductor which emerges from an onsite correlation-driven Mott insulating state and in which the molecular nature of the electronic states gives strong local Jahn-Teller coupling may indicate that the fullerides are indeed non-BCS but are distinct from other examples of unconventional superconductivity in correlated materials.

Methods

Sample. All measurements were performed on a Cs₃C₆₀ sample that contains predominantly f.c.c. (86%) polymorph with secondary A15 Cs₃C₆₀ (3%), body-centred orthorhombic Cs₄C₆₀ (7%) and CsC₆₀ (4%) phases, based on Rietveld refinement of synchrotron powder XRD data¹⁰.

NMR measurements. ¹³C (nuclear spin $I = 1/2$) and ¹³³Cs (nuclear spin $I = 7/2$) NMR spectra and their spin-lattice relaxation times, T_1 , were measured between 4 and 300 K at a magnetic field of 9.39 T. As references, tetramethylsilane (TMS) and CsNO₃ standards were used with corresponding reference frequencies, $\nu(^{13}\text{C}) = 100.5713$ MHz and $\nu(^{133}\text{Cs}) = 52.4609$ MHz, respectively. In the ¹³C NMR lineshape measurements, a Hahn-echo pulse sequence $\pi/2 - \tau - \pi - \tau - \text{echo}$ was used, with pulse length $t_w(\pi/2) = 8$ μs and interpulse delay $\tau = 40$ μs . In the ¹³³Cs NMR experiments, a two-pulse solid-echo sequence $\pi/2 - \tau - \pi/2 - \tau - \text{echo}$ was used, with a pulse length $t_w(\pi/2) = 5$ μs and an interpulse delay $\tau = 50$ μs . The pulse length was optimized for ¹³³Cs nuclei in the high-symmetry octahedral and tetrahedral sites with zero quadrupole frequency (expected for the f.c.c. Cs₃C₆₀ polymorph), which further suppressed the already weak signals of minority phases. For T_1 measurements, the saturation recovery and inversion recovery techniques were both applied.

High-pressure cell. A home-built clamp-type cell design was used for the high-pressure NMR experiments. The cell body was manufactured from non-magnetic Ni-Cr-Al hardened alloy and 1:1 mixture of fluorinert oils FC-770 and FC-70 was used as pressure medium in order to minimize non-hydrostatic conditions. The ruby N₂ luminescence line was measured *in-situ* in order to follow the evolution of pressure inside the cell at each temperature. The unit-cell volume at each temperature and pressure was calculated from the published f.c.c. Cs₃C₆₀ structural, thermal contraction and compressibility data¹⁰. Since the *in-situ* pressure was notably changing during the temperature dependent measurements, all reported pressures are given as those measured at 35 K. The absolute values of pressures are accurate within ± 0.5 kbar.

1. Bednorz, J. G. & Mueller, K. A. Possible High T_c Superconductivity in the Ba-La-Cu-O System. *Z. Phys.* **B64**, 189 (1986).
2. Steglich, F. *et al.* Superconductivity in the Presence of Strong Pauli Paramagnetism: CeCu₂Si₂. *Phys. Rev. Lett.* **43**, 1892 (1979).
3. Jerome, D., Mazaud, A., Ribault, M. & Bechgaard, K. Superconductivity in a synthetic organic conductor (TMTSF)₂PF₆. *J. Phys. Lett.* **41**, 95 (1980).
4. Takahashi, H. *et al.* Superconductivity at 43 K in an iron-based layered compound LaO_{1-x}F_xFeAs. *Nature* **453**, 376 (2008).
5. Uemura, Y. J. Commonalities in phase and mode. *Nat. Mat.* **8**, 253 (2009).
6. Chu, C. W. High-temperature superconductivity: Alive and kicking. *Nat. Phys.* **5**, 787 (2009).
7. Zhao, G. The pairing mechanism of high-temperature superconductivity: experimental constraints. *Phys. Scr.* **83**, 038302 (2011).
8. Ganin, A. Y. *et al.* Bulk superconductivity at 38 K in a molecular system. *Nat. Mater.* **7**, 367 (2008).
9. Takabayashi, Y. *et al.* The Disorder-Free Non-BCS Superconductor Cs₃C₆₀ Emerges from an Antiferromagnetic Insulator Parent State. *Science* **323**, 1585 (2009).
10. Ganin, A. Y. *et al.* Polymorphism control of superconductivity and magnetism in Cs₃C₆₀ close to the Mott transition. *Nature* **466**, 221 (2010).
11. Pennington, C. H. & Stenger, V. A. Nuclear magnetic resonance of C₆₀ and fulleride superconductors. *Rev. Mod. Phys.* **68**, 855 (1996).
12. Gunnarsson, O. Superconductivity in fullerides. *Rev. Mod. Phys.* **69**, 575 (1997).
13. Klupp, G. *et al.* Dynamic Jahn-Teller effect in the parent insulating state of the molecular superconductor Cs₃C₆₀. *Nat. Comm.* **3**, 912 (2012).
14. Tsuei, C. C. & Kirtley, J. R. Pairing symmetry in cuprate superconductors. *Rev. Mod. Phys.* **72**, 696 (2000).
15. Shen, Z.-X. *et al.* Anomalously large gap anisotropy in the a-b plane of Bi₂Sr₂CaCu₂O_{8+ δ} . *Phys. Rev. Lett.* **70**, 1553 (1993).
16. Tanaka, K. *et al.* Distinct Fermi-Momentum-Dependent Energy Gaps in Deeply Underdoped Bi2212. *Science* **314**, 1910 (2006).
17. Xu, Y.-M. *et al.* Fermi surface dichotomy of the superconducting gap and pseudogap in underdoped pnictides. *Nat. Commun.* **2**, 392 (2011).
18. Hirschfeld, P. J., Korshunov, M. M. & Mazin, I. I. Gap symmetry and structure of Fe-based superconductors. *Rep. Prog. Phys.* **74**, 124508 (2011).

19. Tycko, R. *et al.* Electronic Properties of Normal and Superconducting Alkali Fullerides Probed by ¹³C Nuclear Magnetic Resonance. *Phys. Rev. Lett.* **68**, 1912 (1992).
20. Stenger, V. A. *et al.* NMR measurement of superconducting-state spin susceptibility in alkali fullerides. *Phys. Rev. B* **48**, R9942 (1993).
21. Kiefl, R. F. *et al.* Coherence peak and superconducting energy gap in Rb₃C₆₀ observed by muon spin relaxation. *Phys. Rev. B* **70**, 3987 (1993).
22. Stenger, V. A., Pennington, C. H., Buffinger, D. R. & Ziebarth, R. P. Nuclear Magnetic Resonance of A₃C₆₀ Superconductors. *Phys. Rev. Lett.* **74**, 1649 (1995).
23. Lof, R. W., van Veenendaal, M. A., Koopmans, B., Jonkman, H. T. & Sawatzky, G. A. Band gap, excitons, and Coulomb interaction in solid C₆₀. *Phys. Rev. Lett.* **68**, 3924 (1992).
24. Akashi, R. & Arita, R. Nonempirical study of superconductivity in alkali-doped fullerides based on density functional theory for superconductors. *Phys. Rev. B* **88**, 054510 (2013).
25. Chakravarty, S., Gelfand, M. P. & Kivelson, S. Electronic Correlation Effects and Superconductivity in Doped Fullerenes. *Science* **254**, 970 (1991).
26. Capone, M., Fabrizio, M., Castellani, C. & Tosatti, E. Colloquium: Modeling the unconventional superconducting properties of expanded A₃C₆₀ fullerides. *Rev. Mod. Phys.* **81**, 943 (2009).
27. Murakami, Y., Werner, P., Tsuji, N. & Aoki, H. Ordered phases in the Holstein-Hubbard model: Interplay of strong Coulomb interaction and electron-phonon coupling. *Phys. Rev. B* **88**, 125126 (2013).
28. Han, J. E., Gunnarsson, O. & Crespi, V. H. Strong Superconductivity with Local Jahn-Teller Phonons in C₆₀ Solids. *Phys. Rev. Lett.* **90**, 167006 (2003).
29. Jeglič, P. *et al.* Low-moment antiferromagnetic ordering in triply charged cubic fullerides close to the metal-insulator transition. *Phys. Rev. B* **80**, 195424 (2009).
30. Ihara, Y. *et al.* NMR Study of the Mott Transitions to Superconductivity in the Two Cs₃C₆₀ Phases. *Phys. Rev. Lett.* **104**, 256402 (2010).
31. Ihara, Y. *et al.* Spin dynamics at the Mott transition and in the metallic state of the Cs₃C₆₀ superconducting phases. *Euro. Phys. Lett.* **94**, 37007 (2011).
32. Stephens, P. W. *et al.* Structure of single-phase superconducting K₃C₆₀. *Nature* **351**, 632 (1991).
33. Sato, N. *et al.* Analysis of ¹³C-NMR spectra in C₆₀ superconductors: Hyperfine coupling constants, electronic correlation effect, and magnetic penetration depth. *Phys. Rev. B* **58**, 12433 (1998).
34. Imai, T., Shimizu, T., Yasuoka, H., Ueda, Y. & Kosuge, K. Anomalous Temperature Dependence of Cu Nuclear Spin-Lattice Relaxation in YBa₂Cu₃O_{6.91}. *J. Phys. Soc. Jpn.* **57**, 2280 (1988).
35. Choi, H. J., Roundy, D., Sun, H., Cohen, M. L. & Louie, S. G. The origin of the anomalous superconducting properties of MgB₂. *Nature* **418**, 758 (2002).
36. Souma, S. *et al.* The origin of multiple superconducting gaps in MgB₂. *Nature* **423**, 65 (2003).
37. Christides, C. *et al.* Neutron-scattering study of C₆₀ⁿ⁻ ($n = 3, 6$) librations in alkali-metal fullerides. *Phys. Rev. B* **46**, 12088 (1992).
38. Wzietek, P. *et al.* NMR study of the Superconducting gap variation near the Mott transition in Cs₃C₆₀. *arXiv:13105529 Cond-Mat* (2013). at <http://arxiv.org/abs/1310.5529>.

Acknowledgments

K.P., M.J.R. and D.A. acknowledge the financial support by the European Union FP7-NMP-2011-EU-Japan project LEMSUPER under contract no. 283214. K.P. and M.J.R. thank the EPSRC for support (EP/K027255 and EP/K027212). D.A. also acknowledges the support of the Institute of Advanced Study (IAS) and Chemistry Department, Durham University through the award of a Durham International Senior Research Fellowship. K.P. is a Royal Society Wolfson Research Merit Award holder and M.J.R. is a Royal Society Research Professor.

Author contributions

K.P., M.J.R. and D.A. designed and supervised the project. The samples were synthesized by A.G. and Y.T., who also performed the synchrotron X-ray diffraction and magnetic measurements, and analyzed the data. The NMR experiments were conducted and analyzed by A.P., A.K. and P.J. All authors contributed to the interpretation of the data and to the writing of the manuscript.

Additional information

Supplementary information accompanies this paper at <http://www.nature.com/scientificreports>

Competing financial interests: The authors declare no competing financial interests.

How to cite this article: Potočník, A. *et al.* Size and symmetry of the superconducting gap in the f.c.c. Cs₃C₆₀ polymorph close to the metal-Mott insulator boundary. *Sci. Rep.* **4**, 4265; DOI:10.1038/srep04265 (2014).



This work is licensed under a Creative Commons Attribution-NonCommercial-NoDerivs 3.0 Unported license. To view a copy of this license, visit <http://creativecommons.org/licenses/by-nc-nd/3.0>